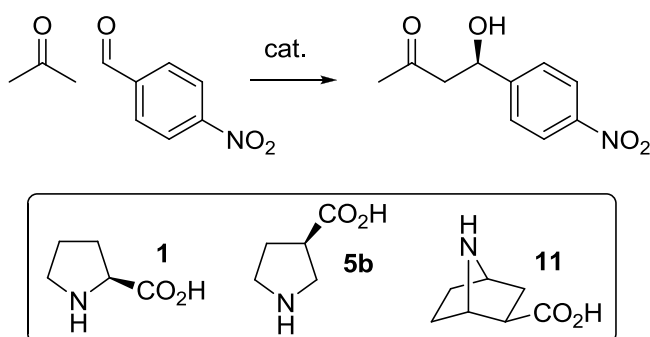# Constrained β-Proline Analogues in Organocatalytic Aldol Reactions: The Influence of Acid Geometry

Alan Armstrong*, Yunas Bhonoah and Andrew J. P. White

Department of Chemistry, Imperial College London, South Kensington, London SW7 2AZ, UK

A.Armstrong@imperial.ac.uk

β-Proline Analogues in Organocatalytic Aldol Reactions

7-Azabicyclo[2.2.1]heptane-2-carboxylic acid **11** was prepared in enantiopure form and its catalytic potential in the direct aldol reaction between acetone and 4-nitrobenzaldehyde assessed. The bicyclic system was found to be more selective than its monocyclic analogue β-proline **5b**. A comparative Density Functional Theory study of proline **1**, β-proline **5b** and **11** in the latter reaction revealed the origin of the improved enantioselectivity of **11** over **5b**. The geometry of the carboxylic acid group in the transition states, which depended critically on pyrrolidine ring conformation, was found to play a key role.

Introduction

Amino acid organocatalysis has received much attention since the discovery in 2000 by List, Lerner and Barbas[1] that proline **1** could catalyse the direct intermolecular aldol reaction (Scheme 1). This seminal work and subsequent efforts have had a significant impact on the organic chemistry community, providing a rapid and efficient approach to the synthesis of chiral molecules.[2] Interestingly, the foundations of the organocatalytic mode of action of proline were laid almost 40 years ago by Hajos and Parrish[3] and, independently, Eder, Sauer and Wiechert,[4] in an intramolecular aldol cyclisation. The scope of transformations that proline can catalyse is truly remarkable and includes the synthetically-important aldol and Mannich reactions; high diastereo- and enantioselectivities are generally observed.

Computational[5-7] and experimental[1,8] studies of the organocatalytic aldol reaction have provided support for a one-proline mechanism based on enamine activation similar to the accepted mechanism for enzymatic aldol reactions (Scheme 2).[1] These investigations have established that the acid functionality is essential for high catalyst activity and selectivity, potentially through hydrogen-bonding activation of the electrophile and stabilisation of the transition states (List-Houk model).[5] An alternative mechanism involving oxazolidinones as product-determining species has recently been proposed by Seebach, Eschenmoser and colleagues;[9] in this model, the electrophile is postulated to approach *anti* to the carboxylic acid group without any hydrogen-bonding activation from the organocatalyst (Scheme 2).

Scheme 1. Proline-Catalysed Intermolecular Aldol Reaction
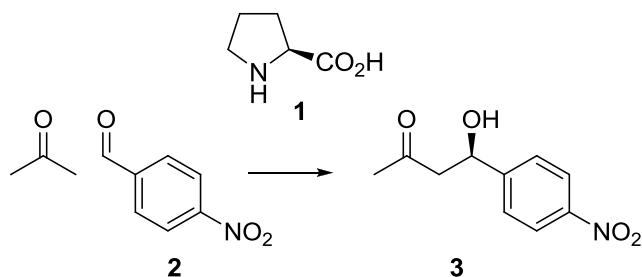
Scheme 2. Proposed Mechanisms of Proline Catalysis
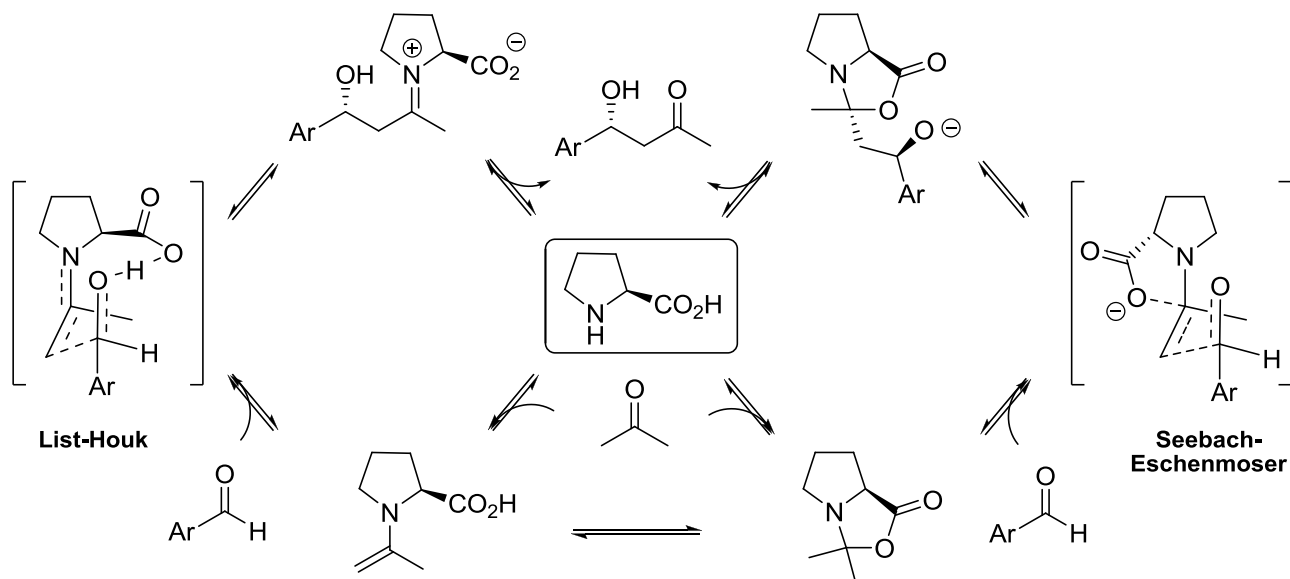
Most investigations into the development of novel amino acid organocatalysts have focused on derivatising the proline scaffold.[2] Studies on other scaffolds, especially where the pyrrolidine ring has been constrained or the spatial relationship between the amine and acid functionalities modified (e.g. β-amino acids), are less common. A selection of such catalysts is shown in Figure 1.[10] Importantly, β-amino acids have shown remarkable selectivity differences to proline-derived catalysts, e.g. β-proline **5b** promotes the classic organocatalytic Mannich reaction with high *anti* diastereoselectivity[10c] while proline provides predominantly the *syn* product.[11] *Cis*-pentacin **8** has been successfully employed in the intramolecular aldol cyclisation to generate the opposite enantiomeric product compared to the proline-catalysed reaction.[10f] Applications of β-amino acids to the direct intermolecular aldol reaction remain limited.[10e,12]
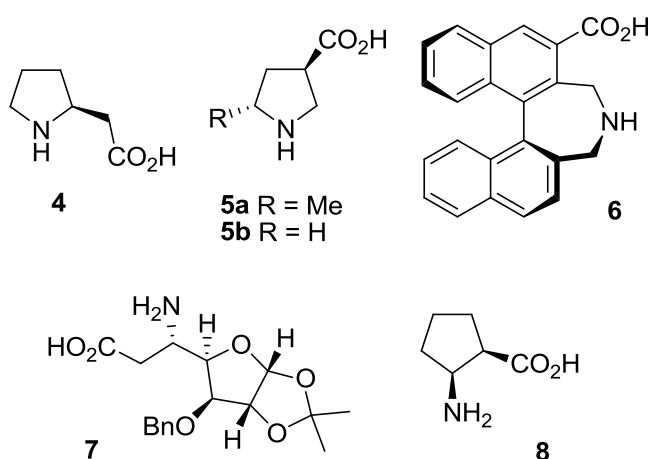
Figure 1. Constrained or β-Amino Acids Employed in Organocatalysis

Our group has recently reported the preparation of constrained β-proline analogue *rac*-**10**[13] by an aza-Prins-pinacol rearrangement strategy[14] and we wondered whether the free β-amino acid would be capable of promoting organocatalytic reactions in a similar manner to proline (Scheme 3). We envisaged that the structural constraints imposed by the bicyclic system may lead to better organisation of the transition state and consequently influence reaction stereoselectivity. In their study of 4,5-methanoprolines, Hanessian and Houk[15] indeed found that constraints on the pyrrolidine ring impacted upon the planarity of the iminium species formed during the intramolecular aldol reaction and hence affected the enantiomeric excess of the final product. The β-disposition of the carboxylic acid group on our system should also eliminate catalyst decomposition *via* irreversible decarboxylation, a common side reaction plaguing proline-catalysed aldol reactions.[8c] Furthermore, we anticipated that the bicyclic amino acid would have somewhat better solubility than proline in solvents commonly employed in organocatalysis. To the best of our knowledge, there have been no reports on the use of amino acids based on the 7-azabicyclo[2.2.1]heptane motif in organocatalysis, although Shinisha and Sunoj[16] recently disclosed a DFT study of [2.2.1] and [2.1.1] bicyclic α-amino acids in the classic organocatalytic aldol reaction. The calculations predicted higher stereoselectivities than proline, although experimental verification remains to be undertaken.

**Scheme 3. Synthetic Approach to Constrained β-Proline Analogues**
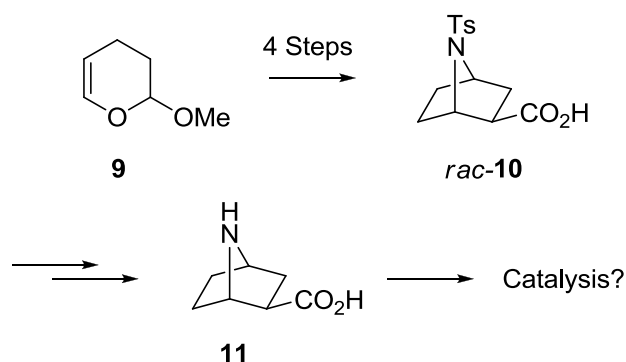
Results and Discussion

1. Catalyst Synthesis

We previously reported the preparation of *N*-Ts acid *rac*-**10**.[13] Our synthetic strategy towards the latter compound cannot easily be rendered asymmetric. We thus initially attempted classical resolution of *rac*-**10** by fractional crystallisation of its diastereomeric salt with various chiral amines.[17] Disappointingly, this proved unsuccessful in providing enantiopure **10**. Covalent attachment of a chiral auxiliary to the racemic acid was more fruitful (Scheme 4); the Evans oxazolidinone diastereomeric adducts **12** and **13** were separable by flash chromatography. Cleavage of the chiral auxiliary from the separated diastereomers gave the desired enantiomerically pure *N*-Ts acids **10** in good yield. The absolute configuration of (1*R*,2*S*,4*S*)-**10** was confirmed by X-ray crystallography (see Supporting Information). Final removal of the tosyl group completed the synthesis of enantiopure bicyclic amino acids **11**.[18]

Scheme 4. Preparation of Enantiopure Bicyclic Amino Acids 11
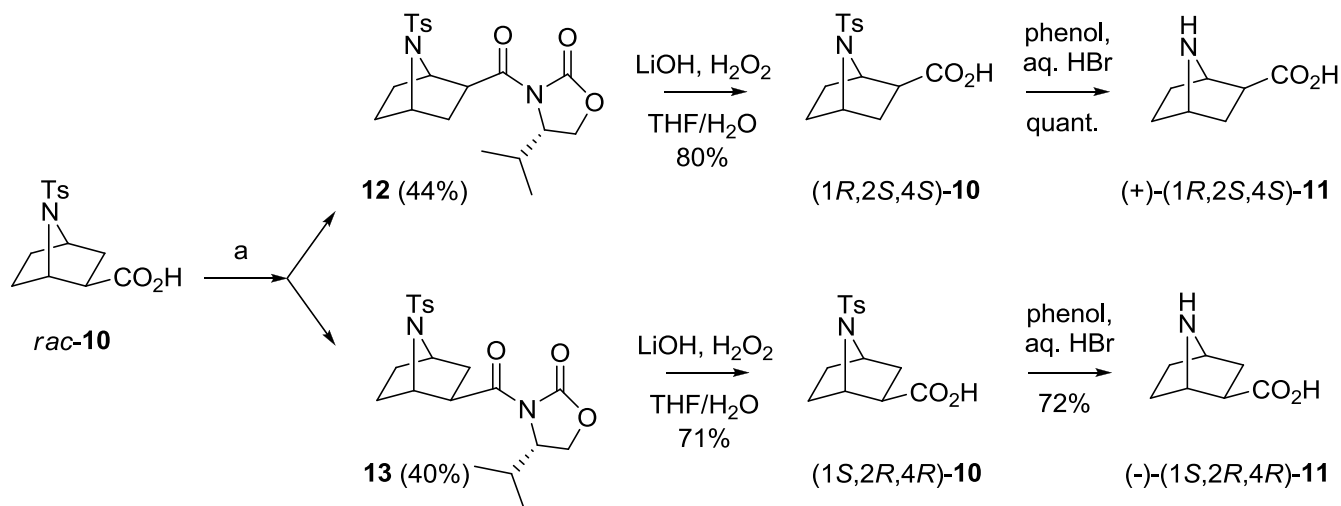
[a] Conditions: (i) Pivaloyl chloride, Et$_3$N, THF (ii) (*S*)-4-Isopropyl-oxazolidin-2-one, ^{n}BuLi, THF, (iii) Flash chromatography

2. Catalyst Assessment

There have been no reports on the use of β-proline **5b** in the direct aldol reaction between acetone and 4-nitrobenzaldehyde, although Barbas and colleagues[10c] have shown that this amino acid is a highly efficient catalyst for the anti-selective Mannich reaction. We assessed the catalytic potential of **5b** in the aldol reaction shown in Scheme 1 in both DMSO and DMF.[19] Whilst good reactivity was observed (Figure 2), we found that β-proline afforded essentially racemic aldol product (Table 1). It was clear that

5

increasing the distance between the secondary amine functionality and the carboxylic acid by an extra carbon has a substantial negative impact on enantioselectivity in the aldol reaction (*c.f.* entries 1 and 2, Table 1), in stark contrast to the organocatalytic Mannich reaction.[10c]
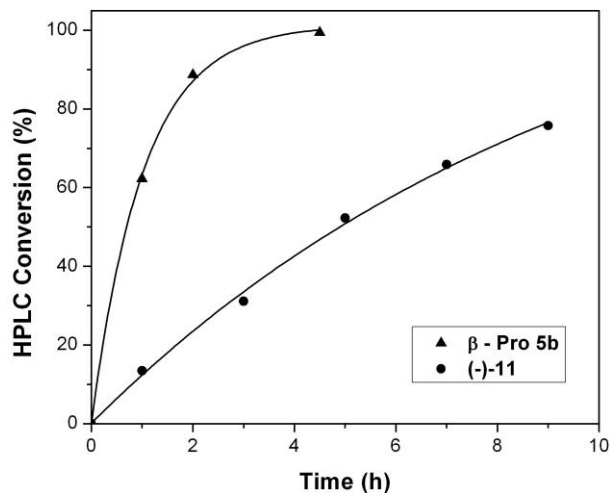

Figure 2. Conversion vs time graphs for the aldol reaction shown in Scheme 1 catalysed by β-proline **5b** or (-)-**11** in DMSO. 20% Catalyst used in all cases.

Table 1. **Observed Enantioselectivities of Aldol Product 3 with Amino Acids 1, 5b and 11**

Entry	Catalyst	Aldol Product *ee* (%)	
		DMSO	DMF
1[a]	Pro **1**	76	76
2	β-Pro **5b**	5	0
3	(-)-**11**	32	40

[a] Proline data from Ref. 1

Having established the effect of changing the position of the carboxylic acid group on enantioselectivity, we turned our attention to the investigation of structural constraints on the pyrrolidine system through the use of optically pure amino acid (-)-**11**. The bicyclic catalyst was found to be slightly less soluble than β-proline as judged by visual inspection and exhibited lower reactivity (Figure 2). Interestingly, the enantiomeric excesses of the aldol product were found to be higher with (-)-**11** than with β-proline, although the former catalyst failed to reach the selectivity levels observed with proline **1** (Table 1). Both (-)-**11** and **1** gave the same sense of asymmetric induction favouring the (*R*)-aldol

6

product, suggesting similar mechanisms of action *via* the List-Houk transition state (Scheme 2).[5] Our aldol results thus show how constraining the pyrrolidine ring of β-proline in a bicyclic framework can have a positive impact on enantiomeric excess (from 0% to 40% *ee* in DMF).[20] This remarkable change in selectivity led us to conduct a comparative study of proline, β-proline and bicyclic amino acid **11** using DFT methods to gain further insight into the nature of the transition states derived from each catalyst.

3. *DFT Study*

Density Functional Theory (DFT) calculations employing the B3LYP functional[21] have been shown to reliably predict product ratios in a variety of proline-catalysed reactions including the aldol, Mannich, aminoxylation and α-alkylation reactions.[6,22] Such studies can also help in the design of novel, more efficient catalysts as evidenced by the work of Barbas, Houk and colleagues[10b] on the use of β-proline analogue **5a** in the *anti* Mannich reaction; DFT studies on **5a** prior to catalyst synthesis predicted selectivities of 95:5 *dr* and 98% *ee*.

Previous computational work on the organocatalytic aldol reaction has revealed that the enantioselectivity is controlled during the C-C bond formation between the enamine intermediate and the aldehyde electrophile.[5,23,24] A key proton transfer from the carboxylic acid group to the developing alkoxide anion helps in stabilising the transition states (TS). Thus the approach of the aldehyde is always *syn* to the acid group. The enamine intermediate can adopt either the s-*cis* or s-*trans* conformation, with the double bond either *syn* or *anti* to the carboxylic acid, respectively. Additionally, the aldehyde offers two prochiral faces (*si* and *re*). In the present study, we have investigated the two enamines (*anti* and *syn*) and four diastereomeric transition states (*anti-re*, *anti-si*, *syn-re* and *syn-si*) for each of the three amino acids in the gas phase and in solvent (Scheme 5). The *anti-re* and *syn-re* structures lead to the *R*-aldol product, while the *anti-si* and *syn-si* TS lead to the enantiomeric *S*-product. Geometry optimisations were performed at the B3LYP level[21] using the 6-31G** basis set.[25] Single point energies were then computed at the same level of theory using the more flexible 6-311+G** basis set.

Scheme 5. Reaction Pathways Studied by DFT
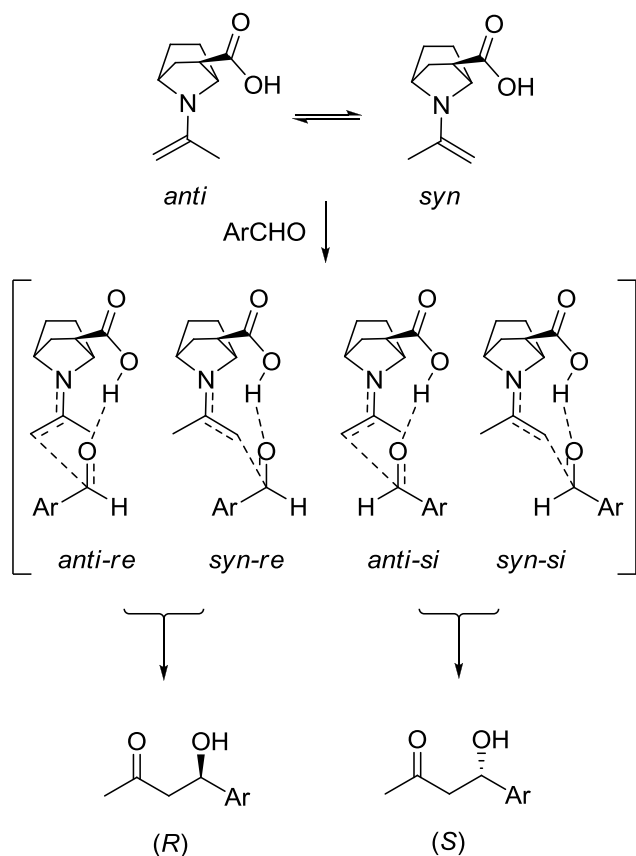
3.1. Proline System

The optimised geometries of the *anti* and *syn* enamines formed between proline and acetone have been previously reported.[24] These were re-optimised at the B3LYP/6-31G** level in the present work and then used for single point energy calculations at higher levels. The computations revealed that the *syn* enamine **14a** was slightly more stable than its *anti* counterpart **14b** seemingly due to steric interactions between the bulkier methyl group and the carboxylic acid in the latter. The enamine nitrogen adopted a nearly planar geometry in both conformers due to favourable overlap of the lone pair with the alkene system (see Supporting Information).[23] Our results were in agreement with those reported previously.[24]

The calculated structures of the four diastereomeric transition states **15a–15d** are shown in Figure 3. Similar theoretical studies have been carried out by Sinisha and Sunoj,[16] although the coordinates of the optimised TS geometries **15a–15d** were not disclosed. Our results paralleled those previously reported for isobutyraldehyde and acetaldehyde acceptor electrophiles.[23,24] Transfer of the carboxyl proton to the alkoxide was observed in all cases; the three atoms engaging in the H-bond were almost co-linear ($\theta =$ 172–173°). We found that transition states derived from the *anti* enamine were more stable than those

8

arising from the *syn* conformer. The *syn-re* and *syn-si* structures **15c** and **15d** tended to have increased pyrrolidine ring puckering as indicated by the data in Figure 3; in these structures, the C3-carbon was out-of-plane, forcing the carboxylic group to adopt a pseudoaxial orientation. Houk and co-workers[5] have shown in similar studies that the *anti* TS are further stabilised by additional weak electrostatic interactions between the partially positive α'-H and the forming alkoxide anion. In our *anti* transition structures, the $NCH^{\delta+}\cdots O^{\delta-}$ distances varied from 2.39 to 2.42 Å. The pseudoequatorial disposition of the aromatic moiety of the aldehyde away from the carboxylic acid group gave rise to an almost completely staggered arrangement around the forming C-C bond in the *anti-re* structure **15a**, making the latter 1.78 kcal/mol lower in energy than the *anti-si* TS **15b** in the gas phase (Table 2). Inclusion of solvent effects led to a stabilisation of all four structures but did not significantly change their relative energies. The product ratio[26] computed from the solvent calculations (92:8) was in good agreement with experimental enantiomeric excesses (76%[1]).
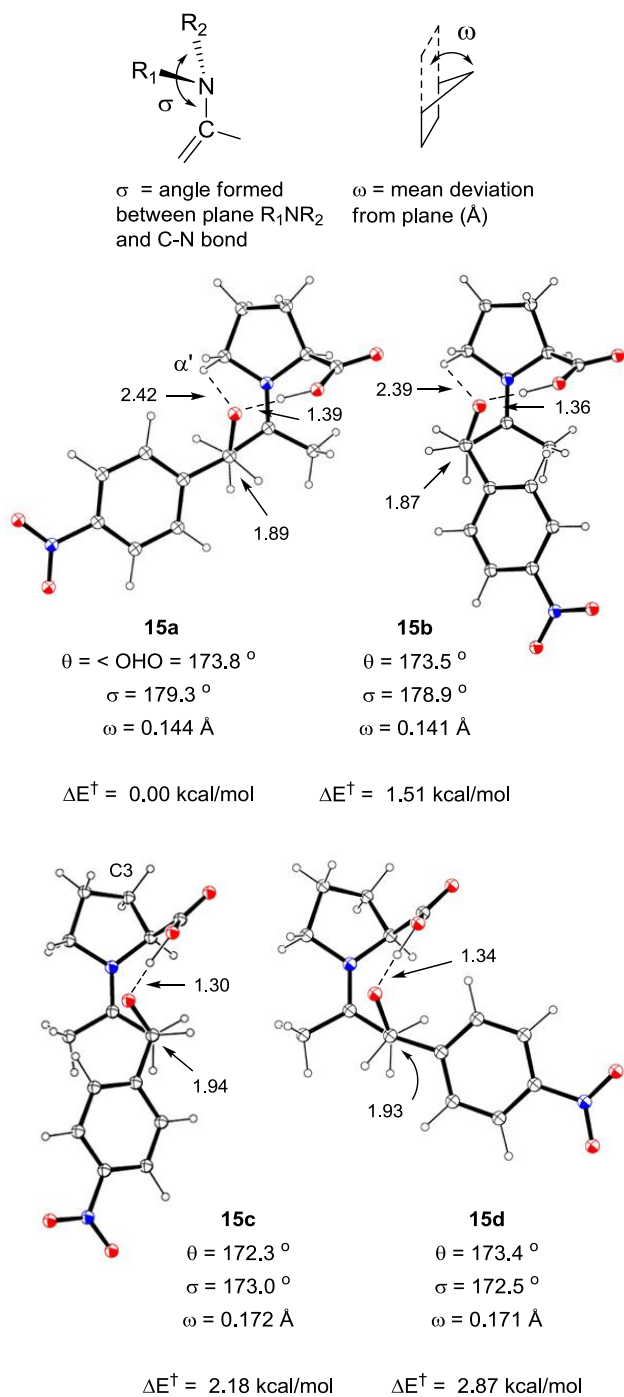
σ = angle formed between plane R_1NR_2 and C-N bond

ω = mean deviation from plane (Å)

15a
θ = < OHO = 173.8 °
σ = 179.3 °
ω = 0.144 Å

ΔE† = 0.00 kcal/mol

15b
θ = 173.5 °
σ = 178.9 °
ω = 0.141 Å

ΔE† = 1.51 kcal/mol

15c
θ = 172.3 °
σ = 173.0 °
ω = 0.172 Å

ΔE† = 2.18 kcal/mol

15d
θ = 173.4 °
σ = 172.5 °
ω = 0.171 Å

ΔE† = 2.87 kcal/mol

Figure 3. B3LYP/6-31G** Optimised TS geometries for the proline-catalysed aldol reaction of Scheme 1. Distances are given in Å. ΔE† values refer to relative energies at $CPCM_{(DMSO)}$/B3LYP/6-311+G**//B3LYP/6-31G**.

Table 2. **Computed Absolute (ΔE_{abs}†) and Relative (ΔE†) Activation Barriers for the Reaction of Scheme 1 at $CPCM_{(DMSO)}$/B3LYP/6-311+G**//B3LYP/6-31G****

Catalyst	TS	$\Delta E_{abs}^{\dagger\ a,\ b}$	$\Delta E^{\dagger\ a,\ b}$
1	**15a**	3.47 (6.37)	0.00 (0.00)
	15b	4.98 (8.15)	1.51 (1.78)
	15c	6.10 (9.18)	2.18 (2.84)
	15d	6.80 (9.62)	2.87 (3.28)
5b	**17a**	11.49 (14.24)	5.54 (2.54)
	17b	6.43 (13.01)	0.48 (1.30)
	17c	6.25 (11.96)	0.06 (0.20)
	17d	6.19 (11.76)	0.00 (0.00)
(-)-11	**19a**	5.84 (8.39)	0.00 (0.00)
	19b	6.63 (10.10)	0.78 (1.72)
	19c	12.02 (15.03)	5.88 (6.56)
	19d	11.05 (13.80)	4.90 (5.33)

[a] Energies in kcal/mol [b] Values in brackets refer to gas phase calculations ($\Delta H_{298abs}^{\dagger}$ and $\Delta H_{298}^{\dagger}$) at B3LYP/6-311+G**//B3LYP/6-31G**

3.2. β-Proline System

The effect of changing the position of the carboxylic acid group was next assessed. Calculated enamine structures of β-proline showed that the *syn* enamine **16a** was also more stable than the *anti* conformer **16b**, although the energy difference was smaller than with proline; no significant interactions were noticed between the enamine and carboxylic groups. As with the proline enamines, a nearly planar nitrogen was observed.

Calculation of the transition state structures **17a–17d** revealed interesting results (Figure 4). To achieve the necessary proximity for proton transfer, three of the four structures (**17a**, **17c** and **17d**) had puckered pyrrolidine rings such that the carboxylic acid-bearing carbon was out-of-plane. Such distortion put the acid group in a pseudoaxial disposition. All four structures showed some electrostatic interaction between the α- or α'-H and the alkoxide anion ($NCH^{\delta+} \cdots O^{\delta-}$ distances = 2.08–2.47 Å), although these were stronger in the *syn* transition states. Iminium planarities were similar to those observed in the proline system, as judged by dihedral angles. However, in contrast to the proline case, transition states arising from the *syn* enamine were more stable. A significant non-ideal geometry of

proton transfer ($\theta = 163°$) was seen in the *anti-re* TS **17a** with increased puckering of the pyrrolidine ring. We believe these factors are responsible for the high energy of the latter structure. Such distortions were not observed with proline, where the *anti-re* TS **15a** was in fact the most stable diastereomeric structure. Steric interactions were also observed between the aromatic portion of the aldehyde and the carboxylic group in the *anti-si* structure **17b**. More interestingly, the energy difference between the lowest transition states **17c** and **17d** with β-proline was only 0.20 kcal/mol in the gas phase (Table 2). Our results thus show that modification of the position of the acid group leads to drastically reduced facial selectivity for the aldehyde. Inclusion of solvent effects led to a stabilisation of all the transition states by 13–17 kcal/mol. Importantly, the *syn–re* TS **17c** was lowered to a greater extent than the *syn-si* structure **17d** such that the energy difference between the two transition states in solvent was very small (0.06 kcal/mol), giving a calculated product ratio of 53:47. This was in remarkable agreement with our experimental enantiomeric excesses (5%). Interestingly, the *anti-si* TS **17b** was found to be only 0.48 kcal/mol higher in energy than the *syn-si* TS **17d** suggesting that it might contribute to the overall *ee*. Consideration of **17b** in the *ee* calculation led to a product ratio of 62:38, still significantly lower than the proline value. Finally, the activation barrier in solvent was higher than that calculated for proline (Table 2). This was partly due to the greater change in pyrrolidine ring conformation required in the β-proline *syn* enamine to achieve the *syn-si* transition state geometry.
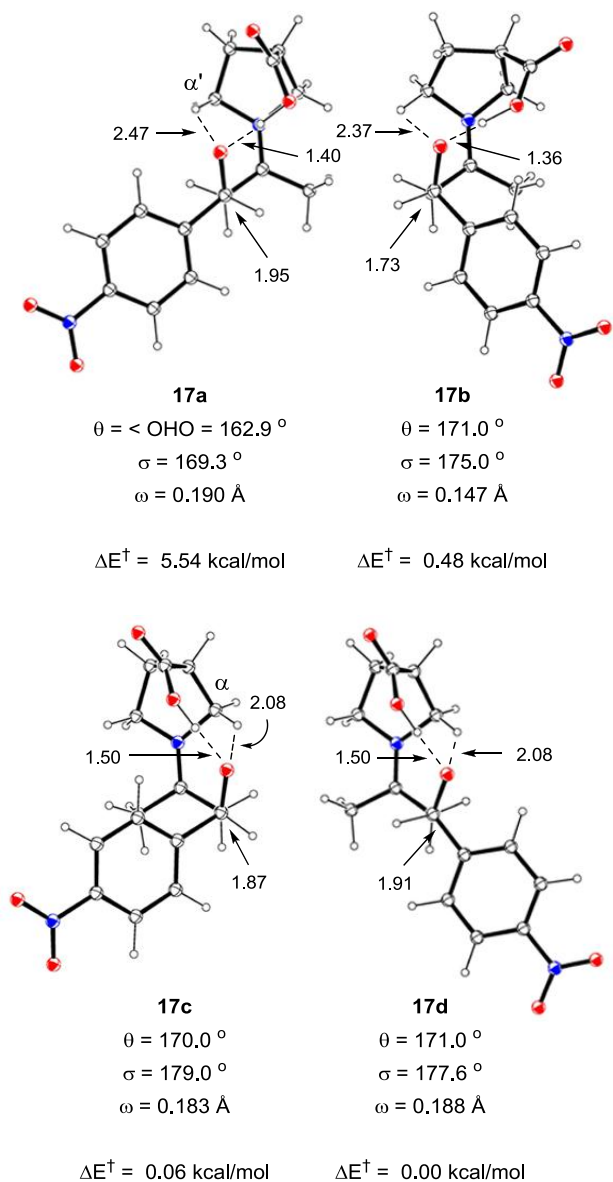
Figure 4. B3LYP/6-31G** Optimised TS geometries for the β-proline-catalysed aldol reaction of Scheme 1. Distances are given in Å. $\Delta E^{\dagger}$ values refer to relative energies at CPCM$_{(DMSO)}$/B3LYP/6-311+G**//B3LYP/6-31G**.

3.3. Bicyclic β-Proline System

With the structural factors responsible for the complete erosion of enantioselectivity with β-proline established, we turned our attention to the study of the effect of constraining the pyrrolidine ring in a [2.2.1] bicyclic system. The calculated structures of the enamines formed by the bicyclic amino acid revealed the *syn* conformer **18b** to be more stable (Figure 5). In stark contrast to the monocyclic

catalysts, the bicyclic enamines were severely pyramidalised at nitrogen (σ = 138°). In both conformers, the disposition of the carboxylic acid proton seemed to suggest intramolecular H-bonding with the bridging nitrogen atom (Figure 5).
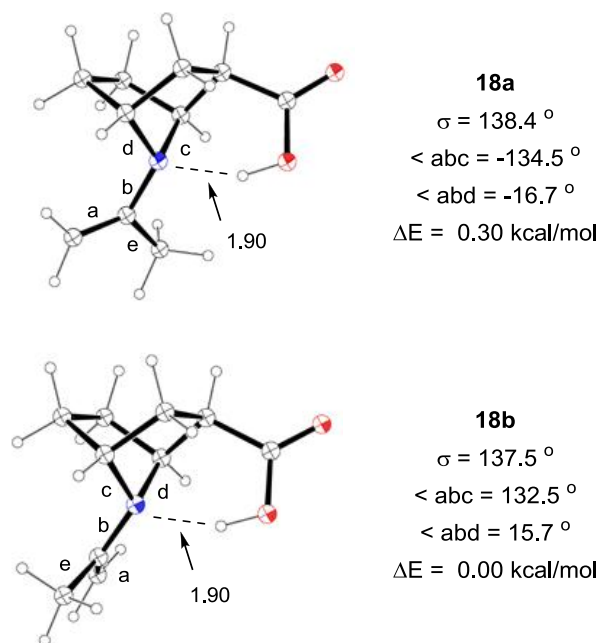

18a
σ = 138.4 °
< abc = -134.5 °
< abd = -16.7 °
ΔE = 0.30 kcal/mol

18b
σ = 137.5 °
< abc = 132.5 °
< abd = 15.7 °
ΔE = 0.00 kcal/mol

Figure 5. B3LYP/6-31G** Optimised enamine structures formed between acetone and amino acid **11**. Distances are given in Å. ΔE values refer to relative energies at CPCM$_{(DMSO)}$/B3LYP/6-311+G**//B3LYP/6-31G**.

The calculated structures of the four diastereomeric transition states **19a–19d** are shown in Figure 6. We found that the structures derived from the *anti* enamine were more stable, analogous to the proline system. The geometry of proton transfer was not ideal for the *syn-re* TS **19c**; severe deviation from linearity was noticed (θ = 163°). Furthermore, no significant interaction was observed between the partially positive α- and β'-hydrogen atoms and the alkoxide anion; these factors account for the high energy of the *syn-re* TS. While the *syn-si* structure **19d** was less prone to these destabilising effects, it suffered from high strain due to distortion of the bicyclic system to achieve ideal proton transfer geometry. This distortion is best illustrated by comparison of the angle λ and the distance between the carboxylic and bridgehead carbon atoms (μ) across the four structures. The destabilisation of *syn-si* was

further augmented by an eclipsing interaction between the carboxylic oxygen and the bridgehead carbon atom.

Analysis of the *anti* structures **19a** and **19b** revealed good geometry for proton transfer in both cases ($\theta = 171°$). Interestingly, the orientation of the carboxylic acid group seemed to be assisted by the axial β-hydrogen. Both transition states enjoyed further stabilisation due to electrostatic interactions between the partially positive β'-hydrogen and the forming alkoxide anion ($CH^{\delta+} \cdots O^{\delta-}$ distances = 2.29–2.33 Å). The *anti-re* structure **19a** was more stable than its *anti-si* counterpart **19b** by 1.72 kcal/mol in the gas phase (Table 2), with a completely staggered arrangement around the forming C-C bond. We attribute the higher energy of the *anti-si* TS to a steric clash between the aromatic fragment and the carboxylic group, along with extra gauche interactions at the forming C-C bond. As with the previous catalysts, the inclusion of solvent effects led to stabilisation of all four transition states (by 14–16 kcal/mol). Interestingly, the energy difference between **19a** and **19b** was considerably reduced (0.78 kcal/mol) compared to the gas phase values. The calculated product ratio in solvent (79:21) was in fair agreement with experimental data (32% *ee*). Greater accuracy can potentially be achieved by conducting full geometry optimisation in the presence of solvent rather than single-point calculations. These have not been carried out in the present study due to their extremely high computational cost. Nevertheless, the DFT results described above successfully rationalise the experimentally-observed trend in selectivity with the three amino acids and show how the accessibility of the various transition states involved in the aldol reaction changes with catalyst modification.
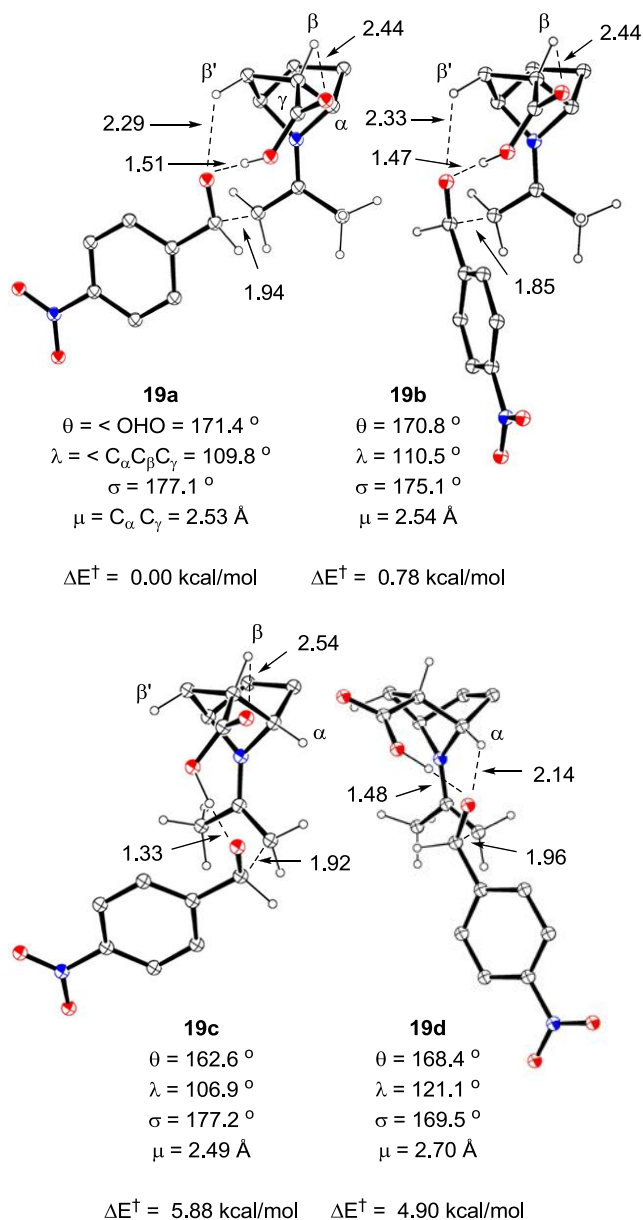
Figure 6. B3LYP/6-31G** Optimised TS geometries for the **11**-catalysed aldol reaction of Scheme 1. Distances are given in Å. Only selected hydrogen atoms shown. $\Delta E^{\dagger}$ values refer to relative energies at $\text{CPCM}_{(\text{DMSO})}$/B3LYP/6-311+G**//B3LYP/6-31G**

Conclusion

Enantiopure amino acid **11** was prepared and its catalytic potential in the direct aldol reaction between acetone and 4-nitrobenzaldehyde assessed. The bicyclic amino acid showed reduced activity compared to its monocyclic analogue β-proline but exhibited greater selectivity, although it failed to reach the levels observed with the natural amino acid proline. DFT calculations revealed that β-proline reacted *via*

its *syn* enamine but exhibited no preference for facial selectivity of the aldehyde. Constraining the β-proline ring in a bicyclic system led to stabilisation of the *anti* transition states compared to the *syn* counterparts. The *anti* enamine was able to differentiate between the two prochiral faces of the aldehyde, although the facial selectivity was reduced when compared to the proline system. Our studies provide the first computational rationalisation of the poor selectivity of β-proline in the classic organocatalytic aldol reaction and show how constraining the pyrrolidine ring can modify the carboxylic acid geometry and contribute towards improving enantioselectivity. We believe that such rigidification strategies can be valuable in the design and development of improved catalysts. The remarkable agreement between the calculated and experimental enantiomeric excesses provides further support for the List-Houk transition state model and emphasises the importance of hydrogen bonding interactions provided by the carboxylic acid group. The Seebach-Eschenmoser model does not implicate such interactions in determining stereocontrol. While we have not carried out calculations on the latter model, it is satisfying that stereocontrol in a large number of carbonyl α-functionalizations has now been shown to be consistent with the List-Houk model. Work is underway in our laboratory to synthesise and study analogues of bicyclic amino acid **11** in the aldol and related reactions.

Experimental Section

(S)–4–Isopropyl–3–((1R,2S,4S)–7–tosyl–7–azabicyclo[2.2.1]heptane–2–carbonyl)oxazolidin–2–one 12 and (S)–4–isopropyl–3–((1S,2R,4R)–7–tosyl–7–azabicyclo[2.2.1]heptane–2–carbonyl)–oxazolidin–2–one 13

To a suspension of *N*–Ts acid *rac*-**10** (1.10 g, 3.73 mmol, 1.0 equiv) in THF (25 mL) at 0 °C was added dropwise triethylamine (0.93 mL, 6.66 mmol, 1.8 equiv) followed by pivaloyl chloride (0.69 mL, 5.55 mmol, 1.5 equiv). The resulting heterogeneous mixture was stirred at 0 °C for 25 min, allowed to warm to RT for 40 min, heated to 40 °C for 30 min and then cooled to −78 °C.

Separately, ^{n}BuLi (2.22 mL, 5.55 mmol, 2.5 M in hexanes, 1.5 equiv) was added to a solution of (S)–4–isopropyl–oxazolidin–2–one (0.717 g, 5.55 mmol, 1.5 equiv) in THF (25 mL) at −78 °C and the resulting viscous mixture stirred at that temperature for 1.5 h. The lithiated oxazolidinone was then

17

added dropwise *via* syringe to the solution of the mixed anhydride prepared above over 30 min. The resulting mixture was maintained at −78 °C for a further 30 min, then allowed to warm to 0 °C for 30 min, then to RT for 1.5 h. Sat. aq. NH$_4$Cl was then added, the solution concentrated and the resulting aqueous residue extracted with EtOAc. Combined organics were washed successively with sat. aq. NaHCO$_3$ and brine, dried (MgSO$_4$) and evaporated under reduced pressure. Flash chromatography (EtOAc:petrol 10:90→35:65, carried out 3 times) afforded the following compounds

The less polar diastereomer **12** (0.663 g, 44%) as a colourless oil: $[\alpha]_D^{21}$ +48.0 (*c.* 1.0, CHCl$_3$); IR (film) 1774, 1700, 1386 cm^{-1}; ^{1}H NMR (400 MHz, CDCl$_3$) δ 7.75 (d, *J* = 8.0 Hz, 2H), 7.24 (d, *J* = 8.0 Hz, 2H), 4.40 (d, *J* = 4.0 Hz, 1H), 4.39–4.36 (m, 1H), 4.25 (t, *J* = 8.5 Hz, 1H), 4.18 (dd, *J* = 9.0, 3.0 Hz, 1H), 4.15 (t, *J* = 4.0 Hz, 1H), 3.49 (dd, *J* = 9.0, 5.0 Hz, 1H), 2.39 (s, 3H), 2.34–2.22 (m, 2H), 1.91–1.83 (m, 2H), 1.73 (dd, *J* = 12.0, 9.0 Hz, 1H), 1.65–1.61 (m, 1H), 1.49–1.45 (m, 1H), 0.88 (d, *J* = 7.0 Hz, 3H), 0.81 (d, *J* = 7.0 Hz, 3H) ppm; ^{13}C NMR (101 MHz, CDCl$_3$) δ 171.2 (C), 154.0 (C), 143.3 (C), 137.7 (C), 129.2 (2 × CH), 127.5 (2 × CH), 63.5 (CH$_2$), 62.0 (CH), 58.8 (CH), 58.5 (CH), 47.9 (CH), 34.4 (CH$_2$), 29.3 (CH$_2$), 29.0 (CH$_2$), 28.0 (CH), 21.4 (CH$_3$), 17.8 (CH$_3$), 14.6 (CH$_3$) ppm; MS (CI) *m/z* 424 (M+NH$_4$$^+$), 407 (M+H$^+$), 317, 310, 204, 132; HRMS calcd for C$_{20}$H$_{27}$N$_2$O$_5$S (M+H$^+$) 407.1641, found, 407.1650.

The more polar diastereomer **13** (0.605 g, 40%) as a colourless oil: $[\alpha]_D^{21}$ +72.0 (*c.* 1.0, CHCl$_3$); IR (film) 1772, 1700, 1387 cm^{-1}; ^{1}H NMR (400 MHz, CDCl$_3$) δ 7.74 (d, *J* = 8.0 Hz, 2H), 7.24 (d, *J* 8.0 Hz, 2H), 4.41–4.37 (d, *J* = 4.0 Hz, 1H), 4.30 (d, *J* = 4.5 Hz, 1H), 4.28 (t, *J* = 4.5 Hz, 1H), 4.24 (t, *J* = 8.0 Hz, 1H), 4.18 (dd, *J* = 9.0, 3.0 Hz, 1H), 3.48 (dd, *J* = 8.5, 5.0 Hz, 1H), 2.55–2.49 (m, 1H), 2.30 (s, 3H), 2.18–2.10 (m, 1H), 2.01–1.93 (m, 1H), 1.90–1.82 (m, 1H), 1.76–1.69 (m, 1H), 1.52–1.47 (m, 2H), 0.85 (d, *J* = 7.0 Hz, 3H), 0.71 (d, *J* = 7.0 Hz, 3H) ppm; ^{13}C NMR (101 MHz, CDCl$_3$) δ 171.0 (C), 154.1 (C), 143.4 (C), 137.7 (C), 129.4 (2 × CH), 127.6 (2 × CH), 63.6 (CH$_2$), 63.4 (CH), 59.2 (CH), 58.5 (CH), 48.0 (CH), 32.4 (CH$_2$), 29.5 (CH$_2$), 29.2 (CH$_2$), 28.4 (CH), 21.5 (CH$_3$), 17.9 (CH$_3$), 14.6 (CH$_3$) ppm;

MS (CI) *m/z* 424 (M+NH$_4$$^+$), 407 (M+H$^+$); HRMS calcd for C$_{20}H_{27}N_2O_5$S (M+H$^+$) 407.1641, found, 407.1646.

(1*R*,2*S*,4*S*)–7–Tosyl–7–azabicyclo[2.2.1]heptane–2–carboxylic acid (1*R*,2*S*,4*S*)–10 and (1*S*,2*R*,4*R*)–7–tosyl–7–azabicyclo[2.2.1]heptane–2–carboxylic acid (1*S*,2*R*,4*R*)–10

To a solution of oxazolidinone **12** (0.663 g, 1.63 mmol, 1.0 equiv) in THF/H$_2$O (4:1, 40 mL) at 0 °C was added H$_2$O$_2$ (1 mL, 9.80 mmol, 30% wt. in H$_2$O, 6.0 equiv) and the resulting mixture stirred for 5 min. A solution of LiOH.H$_2$O (0.137 g, 3.27 mmol, 2.0 equiv) in H$_2$O (10 mL) was then added and the reaction mixture allowed to warm to RT and stirred for 5 h. Na$_2$SO$_3$ (0.6 M, 25 mL) and sat. aq. NaHCO$_3$ (25 mL) were then added and the resulting solution concentrated under reduced pressure. The resulting aqueous residue was washed with chloroform (3 × 30 mL), acidified to pH 1 with 3 M HCl and extracted with EtOAc (4 × 50 mL). The combined EtOAc layers was dried (MgSO$_4$) and evaporated under reduced pressure to give acid (1*R*,2*S*,4*S*)–**10** (0.387 g, 80%) as a white solid: mp 113 °C; [α]$_D^{21}$ 0.0 (*c.* 0.2, CHCl$_3$); IR (nujol) 1700, 1155 cm^{-1}; ^{1}H NMR (400 MHz, CDCl$_3$) δ 9.13 (br s, 1H), 7.79 (2d, *J* = 8.0 Hz, 2H), 7.27 (d, *J* = 8.0 Hz, 2H), 4.52 (d, *J* = 4.0 Hz, 1H), 4.29 (t, *J* = 4.0 Hz, 1H), 2.59 (dd, *J* = 9.0, 5.0 Hz, 1H), 2.42 (s, 3H), 2.29–2.23 (m, 1H), 2.01–1.91 (m, 2H), 1.72 (dd, *J* = 12.0, 9.0 Hz, 1H), 1.51–1.47 (m, 2H) ppm; ^{13}C NMR (101 MHz, CDCl$_3$) δ 178.1 (C), 143.7 (C), 137.3 (C), 129.5 (2 × CH), 127.6 (2 × CH), 61.6 (CH), 58.9 (CH), 47.6 (CH), 34.6 (CH$_2$), 29.3 (CH$_2$), 29.1 (CH$_2$), 21.6 (CH$_3$) ppm; MS (CI) *m/z* 313, 296 (M+H$^+$); HRMS calcd for C$_{14}$H$_{18}$NO$_4$S (M+H$^+$) 296.0957, found, 296.0962. The absolute structure of (1*R*,2*S*,4*S*)–**10** was confirmed by X–ray of a single crystal grown from MeOH/H$_2$O (See Supporting Information).

N–Ts acid (1*S*,2*R*,4*R*)–**10** was prepared using the same procedure as for (1*R*,2*S*,4*S*)–**10**; oxazolidinone **13** (0.605 g, 1.49 mmol, 1.0 equiv), H$_2$O$_2$ (0.91 mL, 8.94 mmol, 30% wt. in H$_2$O, 6.0 equiv), LiOH.H$_2$O (0.125 g, 2.98 mmol, 2.0 equiv). (1*S*,2*R*,4*R*)–**10** (0.312 g, 71%) was obtained as a white solid: mp 178 °C; [α]$_D^{21}$ 0.0 (*c.* 0.2, CHCl$_3$); IR (nujol) 1700, 1155 cm^{-1}; ^{1}H NMR (400 MHz, CDCl$_3$) δ 7.78 (d, *J* = 8.0 Hz, 2H), 7.25 (d, *J* = 8.0, 2H), 4.50 (d, *J* = 4.0 Hz, 1H), 4.27 (t, *J* = 4.0 Hz, 1H), 2.57 (dd, *J* = 9.0,

5.0 Hz, 1H), 2.40 (s, 3H), 2.27–2.21 (m, 1H), 2.01–1.89 (m, 2H), 1.71 (dd, J = 12.0, 9.0 Hz, 1H), 1.54–1.49 (m, 2H) ppm; ^{13}C NMR (101 MHz, CDCl$_3$) δ 178.1 (C), 143.7 (C), 137.3 (C), 129.5 (2 × CH), 127.6 (2 × CH), 61.6 (CH), 58.9 (CH), 47.6 (CH), 34.6 (CH$_2$), 29.3 (CH$_2$), 29.1 (CH$_2$), 21.5 (CH$_3$) ppm; MS (CI) m/z 313 (M+NH$_4^+$), 296 (M+H$^+$); HRMS calcd for C$_{14}$H$_{18}$NO$_4$S (M+H$^+$) 296.0957, found, 296.0961.

(1S,2R,4R)–7–Azabicyclo[2.2.1]heptane–2–carboxylic acid (–)–11 and (1R,2S,4S)–7–azabicyclo[2.2.1]heptane–2–carboxylic acid (+)–11[18]

A mixture of the N–protected amino acid (1S,2R,4R)–**10** (0.700 g, 2.37 mmol, 1.0 equiv) and phenol (0.670 g, 7.12 mmol, 3.0 equiv) was heated under reflux in 48% aq. HBr (20 mL) for 5 h. The reaction mixture was then allowed to cool to RT, diluted with water (20 mL) and extracted with EtOAc. The aqueous layer was separated and evaporated under reduced pressure to give a crude brown solid which was dissolved in H$_2$O and loaded on a Dowex® 50WX8–100 ion–exchange resin (H$^+$ form, activated with 1 M HCl). The loaded resin was washed with distilled water and then eluted with 3 M aq. NH$_3$. The latter fractions were concentrated under reduced pressure, the concentrate then boiled for 5 min with activated charcoal, filtered and the filtrate evaporated under reduced pressure. The resulting semi–solid was dissolved in toluene/MeOH (2:1), the solvent then evaporated and this procedure repeated twice to give amino acid (–)–**11** (0.240 g, 72%) as a white hygroscopic solid: $[\alpha]_D^{21}$ –13.0 (c. 0.77, MeOH), –22.0 (c. 1.0, H$_2$O); IR (ATR) 2956, 2524, 1651, 1562, 1387 cm^{-1}; ^{1}H NMR (400 MHz, CD$_3$OD) δ 4.23 (m, 1H), 4.17 (br s, 1H), 2.62 (t, J = 7.0 Hz, 1H), 2.07–2.05 (m, 2H), 1.94–1.92 (m, 2H), 1.74–1.72 (m, 2H) ppm; ^{13}C NMR (101 MHz, CD$_3$OD) δ 178.9 (C), 62.9 (CH), 59.3 (CH), 47.3 (CH), 34.2 (CH$_2$), 27.6 (CH$_2$), 26.8 (CH$_2$) ppm; MS (CI) m/z 142 (M+H$^+$); HRMS calcd for C$_7$H$_{12}$NO$_2$ (M+H$^+$) 142.0868, found, 142.0871.

Amino acid (+)–**11** was prepared using the same procedure as for (–)–**11**; N–Ts acid (1R,2S,4S)–**10** (0.400 g, 1.36 mmol, 1.0 equiv), phenol (0.383 g, 4.07 mmol, 3.0 equiv), 48% aq. HBr (11 mL). (+)–**11** (0.192 g, quantitative) was obtained as a white hygroscopic solid: $[\alpha]_D^{20}$ +24.0 (c. 1.0, H$_2$O); IR (ATR)

2956, 2535, 1563, 1388 cm^{-1}; ^{1}H NMR (400 MHz, CD$_3$OD) δ 4.23 (m, 1H), 4.17 (br s, 1H), 2.62 (br t, 1H), 2.06–2.04 (m, 2H), 1.94–1.92 (m, 2H), 1.74–1.72 (m, 2H) ppm; ^{13}C NMR (101 MHz, CD$_3$OD) δ 180.0 (C), 63.1 (CH), 59.2 (CH), 48.0 (CH), 34.3 (CH$_2$), 27.8 (CH$_2$), 26.8 (CH$_2$) ppm; MS (CI) m/z 142 (M+H$^+$); HRMS calcd for C$_7$H$_{12}$NO$_2$ (M+H$^+$) 142.0868, found, 142.0871.

Computational Methods

All stationary points (reactants and transition states) were optimized and characterized by frequency analysis using hybrid density functional theory (B3LYP)[21] and the 6-31G**[25] basis set as implemented in Gaussian 03, rev. E.01.[27] The unique imaginary frequencies for the transition states were checked to ensure that the frequency indeed pertained to the desired reaction coordinate. Intrinsic reaction coordinate (IRC)[28] calculations were carried out on selected transition states to verify the energy profile connecting the latter to the two associated minima. Enthalpies at B3LYP/6-31G** were obtained from frequency calculations and include zero-point vibrational energy (ZPVE). Single-point energies were calculated using the more flexible 6-311+G** basis set. Solvation energies for reactants and transition states were computed using a polarisable continuum model (SCRF-CPCM)[29] with a permittivity of 46.7, the value for DMSO, with the united-atom Kohn-Sham (UAKS) radii. All quoted solvation energies refer to the free energy of solvation with all electrostatic terms G$_{solv}^{el}$. These have been previously employed in studies of the organocatalytic aldol reaction.[16] Absolute activation barriers ΔH$_{298abs}$† and ΔE$_{abs}$† (gas-phase and solvent respectively) were obtained as the energy difference between isolated reactants and the corresponding transition state structures. ΔH$_{298}$† values refer to relative gas-phase activation enthalpies and ΔE† values refer to relative activation barriers in DMSO. Enamine starting geometries were initially obtained at AM1 using Spartan ES v.2.0.0.[30] The structures were then optimised at higher levels of theory using Gaussian 03. Measurements of σ (pyramidalisation at nitrogen) and ω (mean deviation from plane) were carried out using Spartan and ChemBio3D Ultra 11.0[31] respectively.

Supporting Information Available: Copies of ^{1}H and ^{13}C-NMR spectra for all new compounds, X-ray crystallographic data (including the CIF) for (1*R*,2*S*,4*S*)-**10**, experimental procedure for the organocatalytic aldol reaction, Cartesian coordinates, electronic energies and selected dihedral angles of all calculated structures, and complete citation for Ref. 27. This material is available free of charge via the Internet at http://pubs.acs.org

References and Footnotes

(1)   List, B.; Lerner, R. A.; Barbas, C. F. *J. Am. Chem. Soc.* **2000**, *122*, 2395-2396.

(2)   Mukherjee, S.; Yang, J. W.; Hoffmann, S.; List, B. *Chem. Rev.* **2007**, *107*, 5471-5569.

(3)   (a) Hajos, Z. G.; Parrish, D. R. German Patent DE 2102623, 1971; (b) Hajos, Z. G.; Parrish, D. R. *J. Org. Chem.* **1974**, *39*, 1615-1621.

(4)   (a) Eder, U.; Sauer, G.; Wiechert, R. German Patent DE 2014757, 1971; (b) Eder, U.; Sauer, G.; Wiechert, R. *Angew. Chem. Int. Ed.* **1971**, *10*, 496.

(5)   Bahmanyar, S.; Houk, K. N.; Martin, H. J.; List, B. *J. Am. Chem. Soc.* **2003**, *125*, 2475-2479.

(6)   Allemann, C.; Gordillo, R.; Clemente, F. R.; Cheong, P. H. Y.; Houk, K. N. *Acc. Chem. Res.* **2004**, *37*, 558-569.

(7)   (a) Bahmanyar, S.; Houk, K. N. *J. Am. Chem. Soc.* **2001**, *123*, 11273-11283; (b) Bahmanyar, S.; Houk, K. N. *J. Am. Chem. Soc.* **2001**, *123*, 12911-12912; (c) Clemente, F. R.; Houk, K. N. *Angew. Chem. Int. Ed.* **2004**, *43*, 5766-5768.

(8)   (a) List, B.; Hoang, L.; Martin, H. J. *Proc. Natl. Acad. Sci. U. S. A.* **2004**, *101*, 5839-5842; (b) Hoang, L.; Bahmanyar, S.; Houk, K. N.; List, B. *J. Am. Chem. Soc.* **2003**, *125*, 16-17; (c) Zotova, N.; Franzke, A.; Armstrong, A.; Blackmond, D. G. *J. Am. Chem. Soc.* **2007**, *129*, 15100-15101; (d) Zotova, N.; Broadbelt, L. J.; Armstrong, A.; Blackmond, D. G. *Bioorg. Med. Chem. Lett.* In Press; (e) Zhu, H.; Clemente, F. R.; Houk, K. N.; Meyer, M. P. *J. Am. Chem. Soc.* **2009**, *131*, 1632-1633.

(9)   Seebach, D.; Beck, A. K.; Badine, D. M.; Limbach, M.; Eschenmoser, A.; Treasurywala, A. M.; Hobi, R.; Prikoszovich, W.; Linder, B. *Helv. Chim. Acta.* **2007**, *90*, 425-471.

(10) (a) Catalyst **4**: Terakado, D.; Takano, M.; Oriyama, T. *Chem. Lett.* **2005**, *34*, 962-963; (b) Catalyst **5a**: Mitsumori, S.; Zhang, H.; Cheong, P. H. Y.; Houk, K. N.; Tanaka, F.; Barbas, C. F. *J. Am. Chem. Soc.* **2006**, *128*, 1040-1041; (c) Catalyst **5b**: Zhang, H. L.; Mitsumori, S.; Utsumi, N.; Imai, M.; Garcia-Delgado, N.; Mifsud, M.; Albertshofer, K.; Cheong, P. H. Y.; Houk, K. N.; Tanaka, F.; Barbas, C. F. *J. Am. Chem. Soc.* **2008**, *130*, 875-886; (d) Catalyst **6**: Kano, T.; Takai, J.; Tokuda, O.; Maruoka, K. *Angew. Chem. Int. Ed.* **2005**, *44*, 3055-3057; (e) Catalyst **7**: Dwivedi, N.; Bisht, S. S.; Tripathi, R. P. *Carbohydr. Res.* **2006**, *341*, 2737-2743; (f) Catalyst **8**: Davies, S. G.; Russell, A. J.; Sheppard, R. L.; Smith, A. D.; Thomson, J. E. *Org. Biomol. Chem.* **2007**, *5*, 3190-3200.

(11) Notz, W.; Tanaka, F.; Watanabe, S.; Chowdari, N. S.; Turner, J. M.; Thayumanavan, R.; Barbas, C. F. *J. Org. Chem.* **2003**, *68*, 9624-9634.

(12) Limbach, M. *Tetrahedron Lett.* **2006**, *47*, 3843-3847.

(13) Armstrong, A.; Bhonoah, Y.; Shanahan, S. E. *J. Org. Chem.* **2007**, *72*, 8019-8024.

(14) Armstrong, A.; Shanahan, S. E. *Org. Lett.* **2005**, *7*, 1335-1338.

(15) Cheong, P. H. Y.; Houk, K. N.; Warrier, J. S.; Hanessian, S. *Adv. Synth. Catal.* **2004**, *346*, 1111-1115.

(16) Shinisha, C. B.; Sunoj, R. B. *Org. Biomol. Chem.* **2007**, *5*, 1287-1294.

(17) Amines used include (*R*)-1-phenylethylamine, (*R*)-1-p-tolylethylamine, (*R*)-1-(4-methoxyphenyl)ethylamine, (*R*)-1-phenylpropylamine, (*R*)-1-(naphthalen-2-yl)ethylamine, (1*R*,2*S*)-2-(dimethylamino)-1-phenylpropan-1-ol, (-)-cinchonidine and quinidine.

(18) Our optical rotation data for (-)-(1*S*,2*R*,4*R*)-**11** was not in agreement with that previously reported for its enantiomer (1*R*,2*S*,4*S*)-**11** by Pandey, G.; Laha, J. K.; Lakshmaiah, G. *Tetrahedron* **2002**, *58*, 3525-3534 ($[\alpha]_D^{25}$ -5.27 (*c*. 1.2, MeOH)). These workers prepared the latter compound *via* an asymmetric [3+2] cycloaddition involving Oppolzer's acryloyl sultam but did not provide proof of the absolute configuration of (1*R*,2*S*,4*S*)-**11**. We can only assume that they derived the stereochemistry from models for facial selectivity of the dienophile as put forward by Curran, D. P.; Kim, B. H. *Tetrahedron* **1993**, *49*, 293. In our work, the *absolute* configurations of both enantiomers of amino acid **11** are based on the X-ray structure of (1*R*,2*S*,4*S*)-**10**; there is no possibility of racemisation during the deprotection reaction leading to the free amino acid.

(19) β-Proline **5b** was obtained from its commercial N-Boc derivative following deprotection with TFA, see Zhang, H. L.; Mifsud, M.; Tanaka, F.; Barbas, C. F. *J. Am. Chem. Soc.* **2006**, *128*, 9630-9631.

(20) Other solvents attempted with amino acid (-)-**11** include acetone (36% ee), acetonitrile (34% ee) and NMP (18% ee); the reaction rates in these were reduced compared to DMSO and DMF.

(21) (a) Becke, A. D. *J. Chem. Phys.* **1993**, *98*, 5648-5652; (b) Lee, C. T.; Yang, W. T.; Parr, R. G. *Phys. Rev. B* **1988**, *37*, 785-789

(22) Fu, A. P.; List, B.; Thiel, W. *J. Org. Chem.* **2006**, *71*, 320-326.

(23) Arno, M.; Domingo, L. R. *Theor. Chem. Acc.* **2002**, *108*, 232-239.

(24) Rankin, K. N.; Gauld, J. W.; Boyd, R. J. *J. Phys. Chem. A* **2002**, *106*, 5155-5159.

(25) Hehre, W. J.; Radom, L.; Schleyer, P. V.; Pople, J. A. *Ab Initio Molecular Orbital Theory*; Wiley, New York., 1986.

(26) Product ratios were calculated using absolute rate theory: ln $(k_1/k_2) = -\Delta\Delta G/RT$. See Ref. 5. Product ratios computed from solvent calculations were in better agreement with experimental data than those derived from gas-phase ($\Delta H_{298}{}^{\dagger}$ and $\Delta G_{298}{}^{\dagger}$) calculations although the same general trend in the energies of the transition states were observed in all cases.

(27) Frisch, M. J., *et al*. *Gaussian 03, Rev. E01*. See Supporting Information for full citation.

(28) (a) Gonzalez, C.; Schlegel, H. B. *J. Chem. Phys.* **1991**, *95*, 5853-5860; (b) Gonzalez, C.; Schlegel, H. B. *J. Chem. Phys.* **1989**, *90*, 2154-2161.

(29) (a) Cances, E.; Mennucci, B.; Tomasi, J. *J. Chem. Phys.* **1997**, *107*, 3032-3041; (b) Cossi, M.; Barone, V.; Cammi, R.; Tomasi, J. *Chem. Phys. Lett.* **1996**, *255*, 327-335.

(30) Spartan ES v. 2.0.0, Wavefunction, Inc., Irvine, CA.

(31) ChemBio3D Ultra 11.0, CambridgeSoft Corporation.